Scientific Reports

https://doi.org/10.1038/s41598-026-37761-y

Article in Press

Multi-response optimization and machine learning-based prediction of straight-groove warm incremental sheet forming of AZ31 magnesium alloy

Received: 3 December 2025

Accepted: 24 January 2026

Published online: 27 January 2026

Cite this article as: Khot A.A., Magdum R.A., Magdum A.R. *et al.* Multi-response optimization and machine learning-based prediction of straight-groove warm incremental sheet forming of AZ31 magnesium alloy. *Sci Rep* (2026). https://doi.org/10.1038/s41598-026-37761-y

Amar A. Khot, Rohit A. Magdum, Anjali R. Magdum, Alemu Workie Kebede & Pandivelan Chinnaiyan

Multi-Response Optimization and Machine Learning-Based Prediction of Straight-Groove Warm Incremental Sheet Forming of AZ31 magnesium alloy

Amar A. Khot[1], Rohit A. Magdum[2]*, Anjali R. Magdum[3], Alemu Workie Kebede[4]*, Pandivelan Chinnaiyan[5]

[1]Department of Mechanical Engineering, Sharad Institute of Technology College of Engineering, Yadrav 416115, Maharashtra, India.

[2]Department of Mechanical Engineering, Kasegaon Education Society's Rajarambapu Institute of Technology, affiliated to Shivaji University, Sakharale, MS-415414, India.

[3]Department of Electronics and computer Engineering, Sharad Institute of Technology College of Engineering, Yadrav 416115, Maharashtra, India.

[4]Department of Mechanical Engineering, Institute of Technology, Debre Markos University, P.O. Box 269, Debre Markos, Ethiopia.

[5] School of Mechanical Engineering, VIT, Vellore 632014, India.

*Corresponding author: Alemu Workie Kebede, Email ID: alemu_workie@dmu.edu.et

Rohit A. Magdum, Email ID: Rmagdum73@gmail.com

Abstract

This study investigates the warm straight-groove incremental sheet forming (ISF) behavior of AZ31 magnesium alloy using an integrated experimental, statistical, and machine learning approach. To test the effect of forming temperature, step-down, spindle speed and feed rate, a Taguchi L27 design was used to study the effect of above variables on forming time and forming force. TOPSIS multi-response optimization was used to find the most balanced parameter combination to result in low force and high process efficiency. The statistical result showed that temperature and step-down were the most prevailing factors that controlled the deformation behaviour at warm forming conditions. A Random Forest regression model was constructed in order to increase the predictive

ability, and it was able to successfully recreate the trends in the forming time, forming force, and performance index. The fractographic analysis of the fractured wall of the groove proved the presence of a ductile failure mechanism in which voids and localisation of shear dominate. The combined DOE-TOPSIS-ML-SEM analysis offers a very powerful procedure of comprehending and optimizing the warm incremental sheet forming of lightweight AZ31 magnesium alloy.

Keywords: Incremental sheet forming; AZ31 magnesium alloy; Warm forming; TOPSIS; Taguchi method; Multi-response optimization; Random Forest; forming force; Machine learning.

1. Introduction

Incremental sheet forming (ISF) has proven to be a flexible and dieless forming technology, whereby it is possible to manufacture customised, low-volume sheet parts by localised plastic deformation under the influence of a stylus-like tool designed and controlled by a CNC machine [1,2]. ISF has proven to be more appealing in aerospace, biomedical, and automotive sectors in comparison to traditional stamping, offering greater geometric flexibility, lower tooling costs, and shorter development cycles. However, conventional cold ISF exhibits inherent limitations that hinder its widespread industrial adoption, particularly for lightweight materials. The process is characterized by low productivity due to the incremental nature of deformation and suffers from significant geometric inaccuracies caused by elastic springback. Furthermore, materials with hexagonal close-packed (HCP) crystal structures, such as the AZ31 magnesium alloy, possess limited slip systems at room temperature. Consequently, subjecting AZ31 to conventional cold ISF results in early fracture and poor surface quality, necessitating the use of heat-assisted (warm) strategies to enhance formability.

In recent reviews, ISF has been identified as a key enabling technology in agile manufacturing, with significant advances made in understanding deformation mechanics, formability limits, and process variants that integrate robotic systems and local heating [3-7,40]. Magnesium alloys, particularly AZ31, are becoming of interest due to their high specific

strength and lightweight characteristics; however, the room temperature formability of the HCP crystal structure is inherently low. Warm ISF has hence been widely explored to activate additional slip systems and enhance ductility. A number of studies on warm ISF and straight-groove incremental forming of AZ31 have shown that forming temperature, step-down, and tool kinematics have a strong effect on formability and force requirements, with optimum temperatures in the range of 200 °C to 300 °C [8-10]. According to Zhang et al., warm continuous-groove forming shows particularly strong improvements in formability and introduces severe changes in the microstructure of AZ31B sheets [11], while robot-assisted hot forming has demonstrated better fracture depth and strain distribution [12]. Despite these developments, systematic design-of-experiments (DOE) based studies of straight-groove warm ISF with multi-response optimisation remain rare. Tribology and surface integrity are also critical to ISF performance [42]; Trzepiecinski et al. underlined that lubrication and contact conditions significantly influence the surface finish in ISF of Magnesium and Aluminium alloys [13]. Similarly, Deokar et al. showed that process parameters affect local stress state, thickness gradient, and geometry of non-axisymmetric components [14]. Detailed surveys continue to identify warm ISF of lightweight alloys as a research priority, particularly the need to better understand process response interactions and optimization schemes [3–7,40].

Taguchi DOE, response surface modeling (RSM), and multi-criteria decision-making (MCDM) approaches are extensively used to optimize ISF processes. Magdum and Chinnaiyan applied a hybrid grey–fuzzy Taguchi approach to warm ISF of AZ31 to optimize formability and surface quality [15]. The Technique for Order Preference by Similarity to Ideal Solution (TOPSIS), an effective MCDM technique, has been widely used in machining and forming processes to convert multiple responses into a single closeness coefficient (CC) for ranking parameter combinations [16-20]. Recent studies have applied hybrid Taguchi–TOPSIS schemes to ultrasonic-assisted ISF, demonstrating its value in multi-objective optimization [21]. While statistical approaches like Taguchi-based Grey

Relational Analysis have effectively optimized parameters such as tool diameter and rotational speed [22, 23], recent trends favor advanced hybrid modeling. Frameworks combining RSM with algorithms like Back-Propagation Neural Networks (BPNN) and Genetic Algorithms (GA) offer robust solutions for predicting critical outcomes like wall angle and surface roughness [24,37]. Furthermore, integrating physical insights such as the impact of ultrasonic vibration on plasticity [25] and the role of thermal history in grain refinement [26, 38, 41,43] into these data-driven models has become essential for mastering the process-structure-property relationships in AZ31 forming. However, TOPSIS has not yet been extensively applied to straight-groove warm ISF of AZ31 to optimize forming time and forming force simultaneously.

To address these process complexities, recent research has increasingly turned to Machine Learning (ML) techniques to capture non-linear process behaviors that analytical models often miss. For instance, Ostasevicius et al. [27] utilized ML methods for real-time process monitoring to detect defects, while Sevšek et al. [39] applied soft computing to correlate process parameters with forming outcomes. Harfoush et al. [28] explored artificial intelligence frameworks to optimize toolpath strategies. More recently, Möllensiep et al. [29] developed Artificial Neural Network (ANN) models to predict geometric accuracy, and Wang et al. [30] implemented learning-based model predictive control to enhance trajectory tracking. Recent literature has focused on integrating intelligence into the ISF workflow; Kurra et al. [31] employed machine learning to predict surface roughness, while Mittal et al. [32] utilized data-driven models to estimate formability limits in anisotropic sheets. In the context of warm forming, Liu et al. [33] demonstrated the efficacy of adaptive control algorithms for temperature regulation, while Li et al. [34] applied ML to optimize cooling strategies for induction-assisted processes. Furthermore, studies by Li et al. [35] and Do et al. [36] have successfully applied predictive modelling to fracture mechanics. While ML-based monitoring has shown promise [27], the prediction of combined responses forming time, forming force, and the

TOPSIS-based closeness coefficient (CC) for warm ISF of AZ31 has not yet been comprehensively investigated.

Previous work by the present authors focused on warm ISF of AZ31 under varying wall angles and hybrid GRA–fuzzy optimization [15]. However, straight-groove forming behavior, multi-response TOPSIS optimization, and ML predictive modeling remain unexplored. Therefore, the objectives of this study are to: (1) investigate straight-groove warm ISF of 1-mm AZ31 sheets using an L27 Taguchi design with four key parameters (temperature, step-down, spindle speed, feed rate); (2) perform multi-response optimization using TOPSIS to determine the optimal forming conditions and validate them experimentally; and (3) develop a Random Forest Regressor model to predict forming time, forming force, and CC, followed by feature importance analysis. This integrated DOE–TOPSIS–ML methodology contributes to developing an efficient, predictive framework for warm ISF of AZ31 magnesium alloy.

2. Materials and Methods

2.1 Experimental Preparation

Experimental studies utilized commercially rolled AZ31 magnesium alloy sheets of same thickness 1mm. AZ31 was used because it has low density, high specific strength and better ductile properties when forming in warm conditions. Chemical composition was in accordance with the ASTM B90 specifications, which includes some 3% wt of Al, 1 %wt of Zn, and some traces of Mn to enhance corrosion resistance. The rectangular blanks of 145 mm x 145 mm were made ready to be straight groove formed. Before forming, the sheet faces were first wiped down using acetone to remove any contamination as well as ensuring uniform frictional behaviour. Every blank was studied in the rolling direction to reduce the effects of anisotropy.

A 10 mm diameter hemispherical component made out of hardened steel and polished to reduce friction was placed on a 3 axis CNC vertical machining centre that could afford tool movement accuracy at every ISF process. Warm forming conditions were generated using a custom-

designed localized electric heating chamber positioned beneath the sheet. Warm ISF is essential for AZ31 magnesium alloy, as its hexagonal close-packed (HCP) crystal structure exhibits limited formability at room temperature. Heating the sheet to 200–250 °C activates additional non-basal slip systems (prismatic and pyramidal), reduces flow stress, and delays fracture onset during incremental deformation.

To ensure accurate force measurements, the experimental setup was designed to thermally isolate the Kistler piezoelectric dynamometer from the heating chamber. A thermal insulating layer was placed between the chamber and the dynamometer, effectively preventing heat transfer and allowing the dynamometer to operate within its temperature specification. No thermal drift or signal deviation was observed during warm forming, confirming that force measurements remained unaffected by the heating system. Although this precision introduces a minor measurement tolerance, the selected experimental levels are separated by a 25 °C interval. This spacing ensures that the thermal regimes remain statistically distinct and non-overlapping, minimizing the impact of measurement error on the comparative analysis of material softening behaviour. The experimental set-up is illustrated in Figure 1.

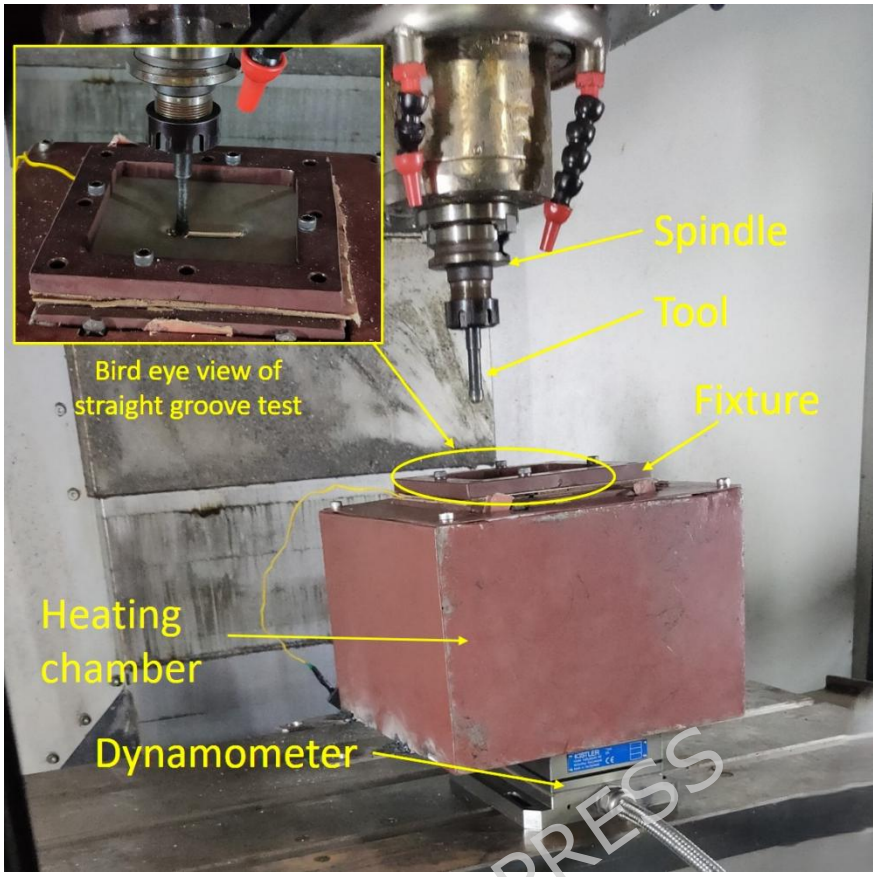

Figure 1. Experimental setup for straight-groove warm ISF.

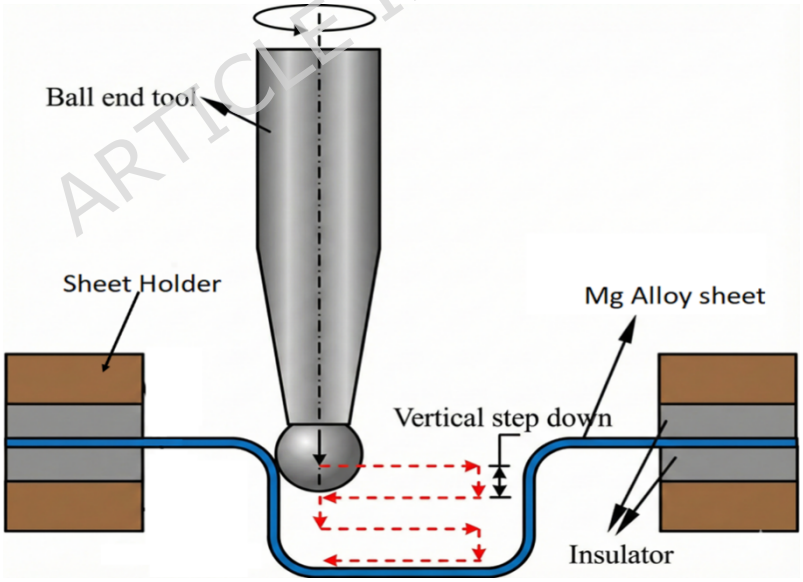

Figure 2. Straight groove test schematic

Straight-groove incremental forming was chosen as the test geometry because it provides controlled deformation and facilitates evaluation of forming force, strain localization, groove depth, and forming time. The programmed groove length was 45 mm, while the groove depth increased

until fracture occurred as shown in Figure 2. Two process responses were measured for each experiment forming time (s) is obtained directly from the CNC controller based on toolpath execution until fracture and Forming Force (N) is measured using a table-mounted piezoelectric dynamometer. These responses are critical for assessing both process productivity and tool–sheet interaction forces.

2.2 Design of Experiments (Taguchi L27 Orthogonal Array)

A Taguchi L27 (3^4) orthogonal array was employed to investigate the influence of four forming parameters at three levels each. The selected control factors were forming temperature, step-down, spindle speed, and feed rate, as summarized in Table 1.

Table 1. Control factors and levels.

Factor	Description	Levels
A	Forming Temperature (°C)	200, 225, 250
B	Step-Down (mm)	0.2, 0.4, 0.6
C	Spindle Speed (rpm)	250, 500, 750
D	Feed Rate (mm/min)	500, 750, 1000

A total of 27 experiments were carried out in a randomized order to minimize systematic bias. The complete design matrix is presented in Table 2, where each trial corresponds to a unique parameter combination. Both forming force and forming time were recorded for subsequent multi-response optimization.

Table 2. L27 experimental design matrix.

Experiment number	Temperature	Step Down	Spindle speed	Feed rate
1	200	0.2	250	500
2	200	0.2	500	750
3	200	0.2	750	1000
4	200	0.4	250	750
5	200	0.4	500	1000
6	200	0.4	750	500
7	200	0.6	250	1000

8	200	0.6	500	500
9	200	0.6	750	750
10	225	0.2	250	500
11	225	0.2	500	750
12	225	0.2	750	1000
13	225	0.4	250	750
14	225	0.4	500	1000
15	225	0.4	750	500
16	225	0.6	250	1000
17	225	0.6	500	500
18	225	0.6	750	750
19	250	0.2	250	500
20	250	0.2	500	750
21	250	0.2	750	1000
22	250	0.4	250	750
23	250	0.4	500	1000
24	250	0.4	750	500
25	250	0.6	250	1000
26	250	0.6	500	500
27	250	0.6	750	750

2.3 Multi-Response Optimization Using TOPSIS

The TOPSIS was used to simultaneously minimize forming time and forming force. TOPSIS ranks alternatives based on their relative closeness to an ideal best solution (minimum force and minimum time) and farthest distance from an ideal worst solution.

The following steps were used:

(1) Normalization

For each response:

$$r_{ij} = \frac{x_{ij}}{\sqrt{\sum_{k=1}^{n} x_{kj}^2}}$$

Where:
i = experiment number, j = response (forming time or forming force), k = all experiments (1 to 27)

(2) Weighted Normalized Matrix: The weighted normalized decision matrix is calculated by multiplying the normalized scores by their associated weights (w_j). In this study, equal weightages ($w_1 = 0.5$, $w_2 = 0.5$) were assigned to forming time and forming force, respectively. This weighting assumption was selected to assign equal importance to process efficiency (time) and mechanical load (force). This assumption is based on the

premise that both responses contribute simultaneously to the warm ISF process performance: forming time reflects process productivity, whereas forming force reflects process mechanics and energy demand. By using equal weights, the optimization objective is to identify a balanced parameter set that minimizes cycle time without allowing excessive forming forces, thereby ensuring a trade-off that favors both productivity and tool/machine safety.

$$v_{ij} = w_j r_{ij}$$

(3) Ideal Best and Ideal Worst

For lower-the-better responses:

$$A_j^* = \min(v_{ij}),$$

$$A_j^- = \max(v_{ij})$$

(4) Separation Measures

Distance from ideal best:

$$S_i^+ = \sqrt{\sum_{j=1}^{m} \left(v_{ij} - A_j^*\right)^2}$$

Distance from ideal worst:

$$S_i^- = \sqrt{\sum_{j=1}^{m} (v_{ij} - A_j^-)^2}$$

(5) Closeness Coefficient (CC)

$$CC_i = \frac{S_i^-}{S_i^- + S_i^+}$$

2.4 Predictive Modelling Using Random Forest Regressor

In order to supplement the experimental analysis, as well as in order to allow predictive understanding of the behaviour of warm ISF, a Random Forest Regressor (RFR) model was created. Figure 3 shows the machine-learning workflow.

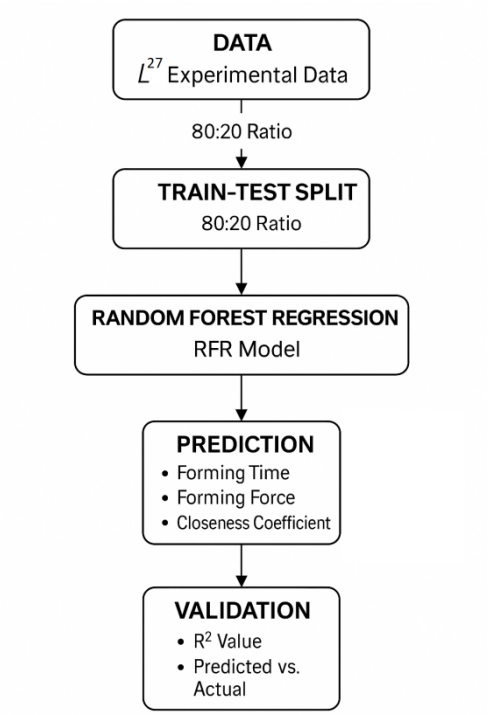

Figure 3. Machine Learning Workflow for ISF response prediction.

A supervised regression model using the Random Forest Regressor (RFR) was developed. RFR is an ensemble learning method that operates by constructing a multitude of decision trees during training. It employs 'bagging' (bootstrap aggregation), where multiple subsets of the original data are created with replacement. For each subset, a decision tree is grown, and the final prediction is obtained by averaging the output of all individual trees. This ensemble approach reduces the risk of overfitting associated with single decision trees and improves prediction accuracy on non-linear datasets like ISF process windows**.** The L27 dataset was split into an 80:20 training–testing ratio. Hyperparameter tuning was performed using a grid-search approach combined with 5-fold cross-validation to avoid overfitting and to ensure model generalization. The tuning search space included number of estimators are around 50–300, maximum tree depth: 5–12, minimum samples per split: 1–6, minimum samples per leaf: 1–4. The optimal hyperparameters were identified as: 200 estimators, a maximum depth of 10, min_samples_split of 2, and min_samples_leaf of 1.

Cross-validation was performed on the training set, and final performance was evaluated on the test set using R^2, mean absolute error (MAE), and root mean square error (RMSE). This ensured that model selection was based on generalization ability rather than training accuracy alone. The model forecasted forming time (s), forming force (N) and the proximity coefficient obtained using TOPSIS. The values of feature-importance obtained by the model provided a strong emphasis on the forming temperature and step-down as the most important predictors of all the responses, which is in agreement with the trends that were generated by ANOVA.

3. Results and Discussion

3.1 TOPSIS Multi-Response Optimization

The warm ISF process performance was evaluated using two major response variables which included forming time and forming force measured in all 27 experiments in the L27 orthogonal array. Forming time is used to indicate the productivity of the process and forming force is used to indicate the resistance to deformation, the tool-sheet interaction and the thermal softening behaviour of AZ31 at higher temperature.

The Technique of Order Preference by Similarity to Ideal Solution (TOPSIS) was used to obtain one multi-response performance measure. The experiments were ordered in terms of their closeness to the ideal best (minimum time and minimum force) and how far they were to the ideal worst (maximum time and maximum force). Table 3 tabulates the normalised values, weighted normalised matrix, the separation distances, the final rankings and the closeness coefficients (CC).

Table 3. TOPSIS optimization results ranking the experimental trials.

Sr. No.	Normalized value		Weighted normalized value		Separation measures		CC	Rank
	Forming time	Forming Force	Forming time	Forming Force	S_plus	S_minus		
1	0.2700	0.1616	0.1350	0.0808	0.0384	0.0389	0.5038	8

2	0.2607	0.1731	0.1304	0.0865	0.0372	0.0335	0.4738	12
3	0.2468	0.1818	0.1234	0.0909	0.0349	0.0311	0.4715	13
4	0.2491	0.2077	0.1245	0.1039	0.0460	0.0190	0.2925	26
5	0.2468	0.2048	0.1234	0.1024	0.0441	0.0209	0.3209	25
6	0.2421	0.2193	0.1211	0.1096	0.0494	0.0172	0.2587	27
7	0.2142	0.2308	0.1071	0.1154	0.0510	0.0283	0.3568	23
8	0.2142	0.2395	0.1071	0.1197	0.0553	0.0279	0.3358	24
9	0.2095	0.2366	0.1048	0.1183	0.0536	0.0303	0.3612	22
10	0.2607	0.1500	0.1304	0.0750	0.0319	0.0450	0.5849	5
11	**0.2421**	**0.1558**	**0.1211**	**0.0779**	**0.0246**	**0.0441**	**0.6415**	**1**
12	0.2491	0.1760	0.1245	0.0880	0.0336	0.0334	0.4985	9
13	0.2374	0.1818	0.1187	0.0909	0.0320	0.0331	0.5091	7
14	0.2351	0.1933	0.1176	0.0966	0.0362	0.0289	0.4441	20
15	0.2165	0.2048	0.1082	0.1024	0.0384	0.0319	0.4537	18
16	0.2212	0.2193	0.1106	0.1096	0.0459	0.0264	0.3654	21
17	0.2118	0.2077	0.1059	0.1039	0.0394	0.0331	0.4570	17
18	0.2002	0.2019	0.1001	0.1010	0.0361	0.0396	0.5236	6
19	0.2700	0.1298	0.1350	0.0649	0.0349	0.0548	0.6109	2
20	0.2607	0.1442	0.1304	0.0721	0.0311	0.0478	0.6059	3
21	0.2468	0.1587	0.1234	0.0793	0.0274	0.0420	0.6055	4
22	0.2491	0.1818	0.1245	0.0909	0.0357	0.0307	0.4626	16
23	0.2468	0.1789	0.1234	0.0894	0.0338	0.0325	0.4897	10
24	0.2421	0.1846	0.1211	0.0923	0.0345	0.0308	0.4714	14
25	0.2142	0.2019	0.1071	0.1010	0.0367	0.0336	0.4781	11

26	0.2142	0.2048	0.1071	0.1024	0.0381	0.0329	0.4628	15
27	0.2095	0.2106	0.1048	0.1053	0.0407	0.0335	0.4519	19

The range of values of the CC, across the 27 trials, was 0.2587 to 0.6415, which showed a great amount of variance in multi-response performance. Experiment 11 (225 °C, 0.2 mm step-down, 500 rpm, 750 mm/min) achieved the highest CC value of 0.6415. This signifies that among the 27 discrete trials, this parameter combination had the shortest Euclidean distance to the ideal best solution (minimum time and minimum force) and the farthest distance from the ideal worst. While 250 °C typically yields the lowest forming force due to maximum thermal softening, Experiment 11 (at 225 °C) provided a superior aggregate score by balancing the trade-off between force reduction and process time more effectively than the specific 250 °C combinations present in the L27 array. This was the best mix of low forming time, and low forming force between the experimental conditions. Though 250 °C is the temperature typically linked with increased ductility, the combination of step-down and spindle rate in the Trial 11 created a more productive inflow of material and a decreased force, which allowed it to overtake all other experiments involving L27.

3.2 Taguchi Response Table for CC

The values of mean Closeness Coefficient (CC) at every level of factors were calculated through the Taguchi L27 orthogonal array to determine the best values of the ISF parameters. Table 4 shows the Taguchi response table, the mean CC values of which are the combined performance of forming time and forming force following TOPSIS normalisation. As can be seen in the analysis, the most significant attributes are Step-down and Forming Temperature the highest Delta values (0.1438 and 0.1404, respectively). On the other hand, Spindle speed and feed rate have relatively smaller Delta values, which suggests that they have a relative insignificance on the overall process performance.

Table 4. Response table

Factor	Level 1	Level 2	Level 3	Delta	Rank
Temperature (°C)	0.3750	0.4975	**0.5154**	0.1404	2
Step-Down (mm)	**0.5552**	0.4114	0.4214	**0.1438**	1
Spindle Speed (rpm)	0.4627	**0.4702**	0.4551	0.0151	4
Feed Rate (mm/min)	0.4599	**0.4802**	0.4478	0.0324	3
			Predicted CC = 0.6330		

This analysis demonstrates the value of the hybrid Taguchi–TOPSIS framework: while Experiment 11 was the best observed trial in the initial L27 ranking, the Taguchi response analysis allows us to predict a superior global optimum that lies outside the discrete experimental matrix. According to the higher-the-better-parameter level criterion of CC, the best parameter levels are considered to be: 250 °C forming temperature (Level 3), 0.2 mm step-down (Level 1), 500 rpm of spindle (Level 2) and 750 mm/min feed rate (Level 2). All these levels optimise the CC and give the most optimal balance between low forming force and low forming time. Although this specific combination was not present in the L27 orthogonal array, the Taguchi additive model allows for the prediction of its performance. The predicted Closeness Coefficient (CC_{pred}) was calculated using the additive equation:

$$CC_{pred} = T + \sum \left(A_{opt} - T\right)$$

where T is the overall mean CC and A_{opt} represents the mean CC at the optimal level for each factor. This calculation yielded a predicted CC of 0.6330, indicating a superior theoretical performance compared to the average experimental results.

3.3 Confirmation Experiment

To validate the optimal parameter combination obtained from the Taguchi–TOPSIS approach, a confirmation experiment was performed at the

predicted optimal levels: 250 °C forming temperature, 0.2 mm step-down, 500 rpm spindle speed, and 750 mm/min feed rate. Using the Taguchi additive prediction model, the expected forming responses at these settings were: Predicted forming time 55.44 s, Predicted forming force: 0.493 kN and Predicted closeness coefficient (CC): 0.6330. The confirmation test was conducted under identical conditions, and the experimentally measured responses were forming time is 53 s, forming force: 0.483 kN and closeness coefficient (CC): 0.6435. The comparison between predicted and experimental results is presented in Table 5. The consistently negative deviations (−4.40% for time and −2.03% for force) indicate that the Taguchi additive model slightly overestimates the required process inputs. This is attributed to synergistic parameter interactions at optimal settings which facilitate material flow more effectively than the linear model predicts. Practically, this overestimation serves as a conservative safety margin, ensuring that actual process loads and cycle times remain below the predicted planning limits.

Table 5. Confirmation Experiment Results

Response	**Predicted Value**	**Experimental Value**	**Deviation (%)**
Forming Time (s)	55.44	53	−4.40%
Forming Force (kN)	0.493	0.483	−2.03%
CC	0.6330	0.6435	+1.66%

The error ranges of predicted and experimental responses were less than and not exceeding 5 percent, verifying the usefulness of Taguchi-TOPSIS framework. Crucially, this confirmation value (0.6435) also exceeds the highest CC observed in the initial L27 array (Experiment 11, CC = 0.6415). This demonstrates the primary role of the confirmation experiment: it validates that the hybrid Taguchi–TOPSIS optimization framework successfully identified a 'global' parameter combination superior to any of the discrete experimental trials conducted in the initial design matrix. The synergy of these parameters is the reason why the optimised combination

of parameters performs better. The interpretation of the detailed effects of individual parameters on the forming time and force is carried out in the following sections.

3.4 Effect on Forming Time

The effect that each process parameter had on the forming time was studied through the main-effects plot in Figure 4. The forming time is based on the total amount of time spent in the profile of the straight-groove form, which is controlled by thermal softening, cumulative deformation mechanics and interaction between the tool and the sheet. The steep positive slope for Forming Temperature (Figure 4) indicates that thermal activation is the most effective driver for process improvement. As temperature rises to 250°C, the substantial reduction in flow stress (due to dislocation unpinning and slip system activation) improves the Force sub-score significantly, while the Time sub-score remains unaffected. This 'pure gain' allows the CC to reach its peak.

Effect of Forming Temperature

The forming time in the range of 200 °C to 250 °C decreases monotonically with the rise in temperatures. It is possible to attribute this tendency to inherent deformation processes of AZ31 magnesium alloy. At relatively low temperatures the alloy is relatively strong in yield as only basal slip systems are open. With the increase in temperature, prismatic and pyramidal systems of slips are triggered, thus decreasing the flow stress and making plastic deformation easier. Greater grain boundary mobility and thermal softening reduce the resistance to tool move which consequently hastens tool-path movement. Groove formation therefore goes faster and shortening the total forming time.

Effect of Step-Down

Step down in a very important parameter influencing the forming time more. A decrease in step-down 0.6 mm to 0.2 mm significantly decreases the forming time. Smoother incremental progression, lower instantaneous load, and reduced elastic recovery are obtained with smaller step-downs.

Larger step-downs, in its turn, cause greater local deformation resistance and dwell time due to a more intense tool penetration per step, slowing down the process and increasing the cycle.

Effect of Spindle Speed

There is insignificant impact on the forming time by the spindle speed. Since warm ISF uses a significant amount of external heat as opposed to frictional heating, tool rotation contributes little to the thermal output. As a result, the change in rpm has no significant impact on the flow stress of the material or the capability of the tool to stay in its programmed path and the forming time varies almost identically between all levels.

Effect of Feed Rate

Feed rate has a rather small decreasing effect on forming time because the larger the feed values, the faster is the speed of the tool. However, this effect is not significant as compared to temperature and step-down. The feed rate was not shown to cause instability, chattering, or loss of reliability to the process within the tested range (500-1000 mm/min), hence its impact is not as high as the effect of thermally driven softening or incremental deformation depth.

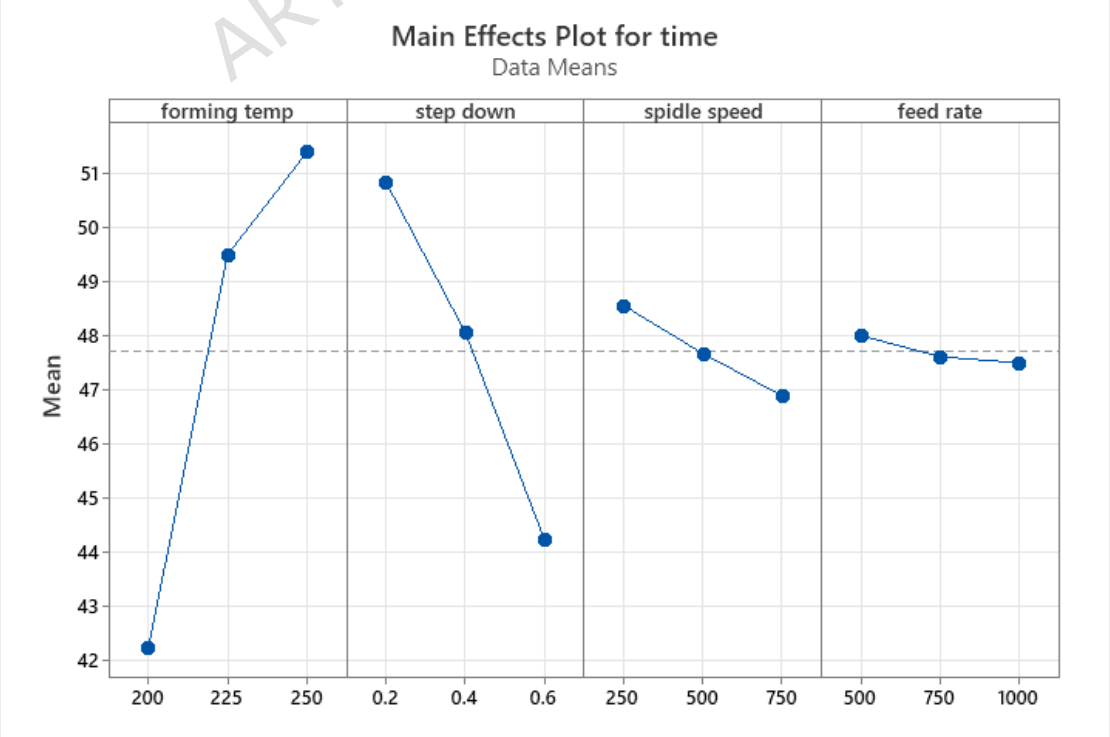

Figure 4. Main effects plot showing the dominant influence of temperature on Forming Time

3.5 Effect on Forming Force

The tendencies in the development of force will be critical towards the understanding of the resistance to deformation, localisation of stresses, and flow of material when warm straight-groove ISF is underway. The main-effects plot that is shown in Figure 5 outlines the comparative impact of the four process parameters on forming force at the peak. The Step-down parameter (Figure 5) reveals a critical trade-off threshold. Although increasing the step-down technically reduces the forming time (a positive input for TOPSIS), the plot shows a sharp decline in CC. This indicates that the 'penalty' incurred from the drastic rise in forming force outweighs the 'reward' gained from shorter cycle times. The steepness of this trend confirms that under the current equal-weighting scheme, the process is mechanically limited; the degradation of tool-sheet interface conditions at higher step-downs negatively impacts the overall closeness to the ideal solution more than the speed gain benefits it.

Effect of Forming Temperature

The rise in temperature results in a strong decrease in forming force. This can be expected because of softening of the thermal effect, decrease in flow stress, activation of more slip systems with high temperatures, a decreased yield point, and increased ductility. There is also a lesser interfacial friction between the hardened surface layers that decrease the resistance to the advancing tool. Together, these decrease the resistance to the progression of the tools, which leads to a significant decrease in the required force.

Effect of Step-Down

Step-down exhibited the most significant direct correlation with forming force. Step-down of 0.2 mm was raised to 0.6 mm and the force demand was significantly augmented. Increasing step-down steps will require more material to be moved per pass, which produces larger localized stresses and increases strain gradient. This results in higher loading of the tools

and more extreme instantaneous deformation making the forming force to shoot up. Larger step-downs increase strain localisation may increase localisation of strain, thinning, and pre-mature fracture, highlighting its importance as an essential process parameter in warm ISF.

Figure 5. Main effects plot highlighting the steep increase in Forming Force with Step-down

Effect of Spindle Speed

The speed of spindle does not influence forming force significantly. The fact that external heating is predominant makes the contribution of friction small and as a result changes in the rotational velocity of the tool have no significant impact on thermal or mechanical conditions of the deformation zone. Thus, the values of the forces are similar in all levels of spindle speed.

Effect of Feed Rate

Feed rate also produces an insignificant influence on forming force. Although feed determines tool motion kinematics, material flow stress and incremental depth are the main factors of deformation behaviour in warm ISF. Feed rate has no significant influence on stress distribution or on the

mode of material flow within the range of test conditions and results in practically identical values of forming forces.

3.6 Analysis of Parameter Interactions and Process Trade-offs

To gain a deeper understanding of the warm ISF mechanics, the influence of experimental parameters on geometric accuracy, productivity, and forming loads was analyzed collectively. This multi-objective perspective highlights the critical trade-offs inherent in the process.

First, the interaction effect on geometric accuracy was investigated. As illustrated in Figure 6, the non-parallel lines indicate a significant interaction between forming temperature and step-down size. At lower temperatures (200°C), increasing the step-down size results in a sharp decline in the Closeness Coefficient (CC), indicating poor geometric fidelity due to increased springback and flow stress. However, at elevated temperatures (250 °C), the slope flattens significantly. This confirms that the thermal softening effect at 250 °C effectively compensates for the mechanical severity of larger step-downs, allowing the process to maintain high geometric accuracy even at aggressive forming rates.

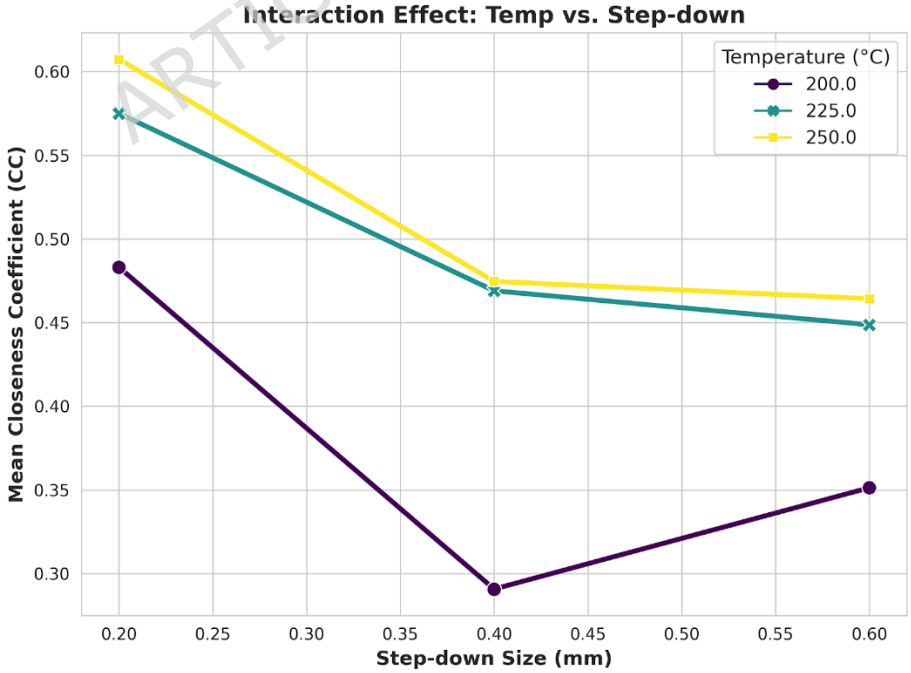

Figure 6. Interaction plot for Closeness Coefficient (CC), showing that higher temperatures (250°C) mitigate the accuracy loss typically caused by large step-downs.

Figure 7 illustrates the distribution of Closeness Coefficient (CC) values across the investigated temperatures. A clear positive trend is observed: at 200°C, the process yields the lowest CC scores with high consistency, whereas 250°C provides the highest median CC value. This indicates that while higher temperatures (225°C and 250°C) increase variability compared to the 200°C baseline, they are essential for achieving the optimal multi-response balance of forming time and force, with 250°C emerging as the superior thermal condition for the TOPSIS optimization.

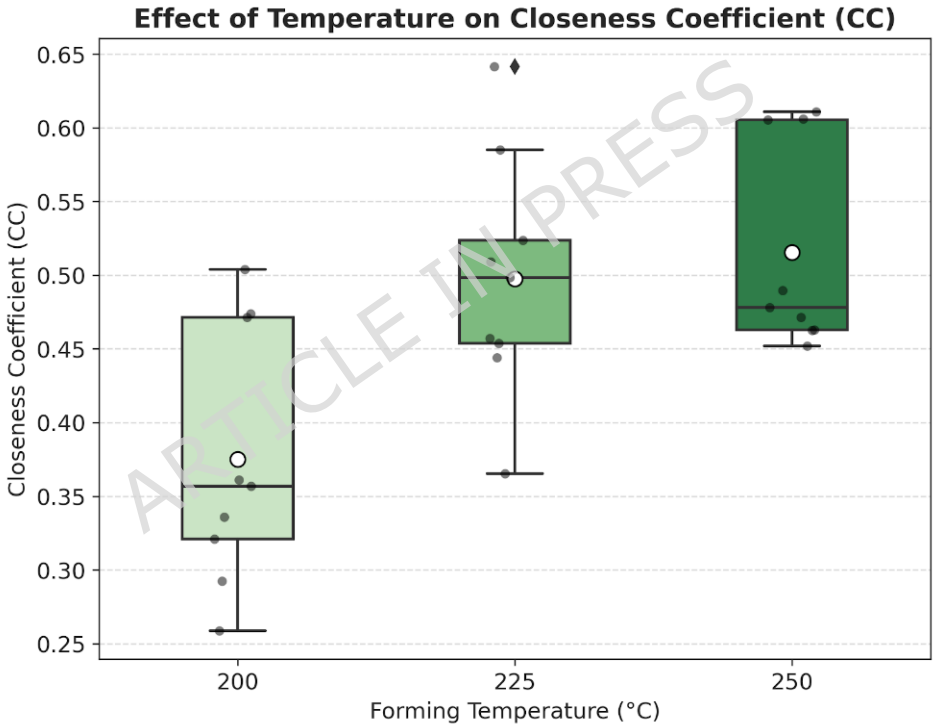

Figure 7. Distribution of Closeness Coefficient (CC) values across different forming temperatures.

To further analyse the interplay between processing parameters, a heatmap of forming temperature versus step-down was generated (Figure 8). The visualization confirms that forming time is highly sensitive to the combination of these two factors. The minimum forming time is achieved at 200°C with a 0.6 mm step-down, represented by the darker region of

the map. Conversely, the maximum processing duration is observed at the 250°C and 0.2 mm step-down condition. This heatmap provides a clear operational map for the AZ31 magnesium alloy, suggesting that while higher temperatures are preferred for multi-response optimization (as shown in the CC analysis), they must be balanced with higher step-down values to maintain temporal efficiency.

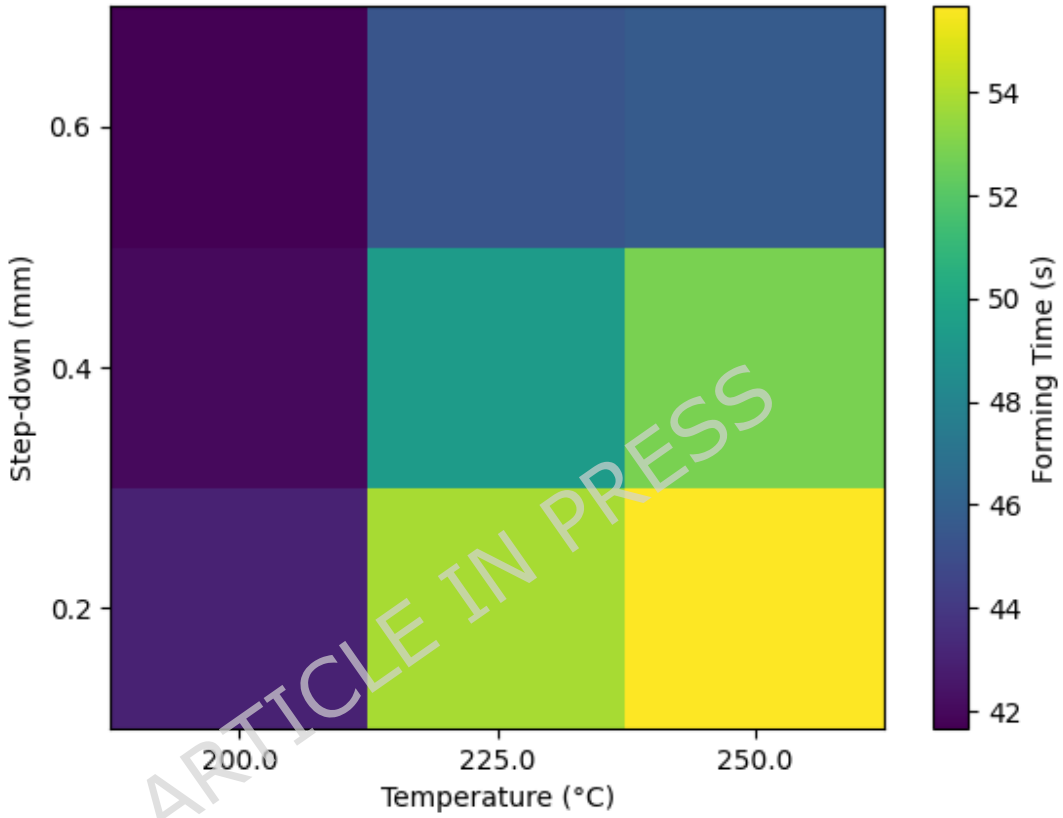

Figure 8. Heatmap illustrating the interaction effect between forming temperature and step-down on the total forming time.

3.7 Fractography Analysis of the Fractured Groove Wall

In order to further explain the mechanism of failure during the process of warm ISF, a scanning electron microscopy (SEM) approach was used to scan the fractured surface of one of the specimens which were developed under the optimal parameter set (250 °C, 0.2 mm step-down, 500 rpm spindle speed, 750 mm/min feed rate). A review of the annotated SEM micrograph in Figure 9 identifies a ductile fracture mode as the dominant mode of fracture, which is said to manifest many deep dimples, tear ridges, and micro-void coalescence.

The big, equiaxed dimples are evidence of high levels of plastic deformation, which proves that the high temperature stimulated the action of more slip systems in AZ31, thus lowering the stress of flow and increasing ductility. There are a number of long tear ridges observed which are in line with the direction of the tool travel that signifies that shearing is localized at each step-down by incremental penetration. This localized shearing is most critical at the maximum fracture depth. As the tool progresses deeper, the wall thickness reduces continuously (cosine law), leading to severe strain accumulation at the groove wall. The SEM analysis confirms that the fracture at this limiting depth is not due to brittle cracking, but rather due to the exhaustion of ductility where the material can no longer sustain the thinning. This behaviour is consistent with the deformation of straight-groove ISF, where the strain is concentrated along the wall of the groove.

Isolated hard particles and oxide inclusions also can be seen, and often serve as nucleation points of micro-void formation, which then increases and unites to large dimples, and the ductile fracture process is then complete. The fact that there is no cleavage facet or brittle plane is supporting that failure is not brittle mode, and it is again supporting the fact that temperature and step-down is the major variable that controls material softening and resistance to deformation. The SEM provides microstructural evidence that is consistent with the previous experimental, TOPSIS, ANOVA, and machine-learned conclusions, which indicates that warm ISF of AZ31 fractures largely by void growth, coalescence, and shear-based ductile fracture.

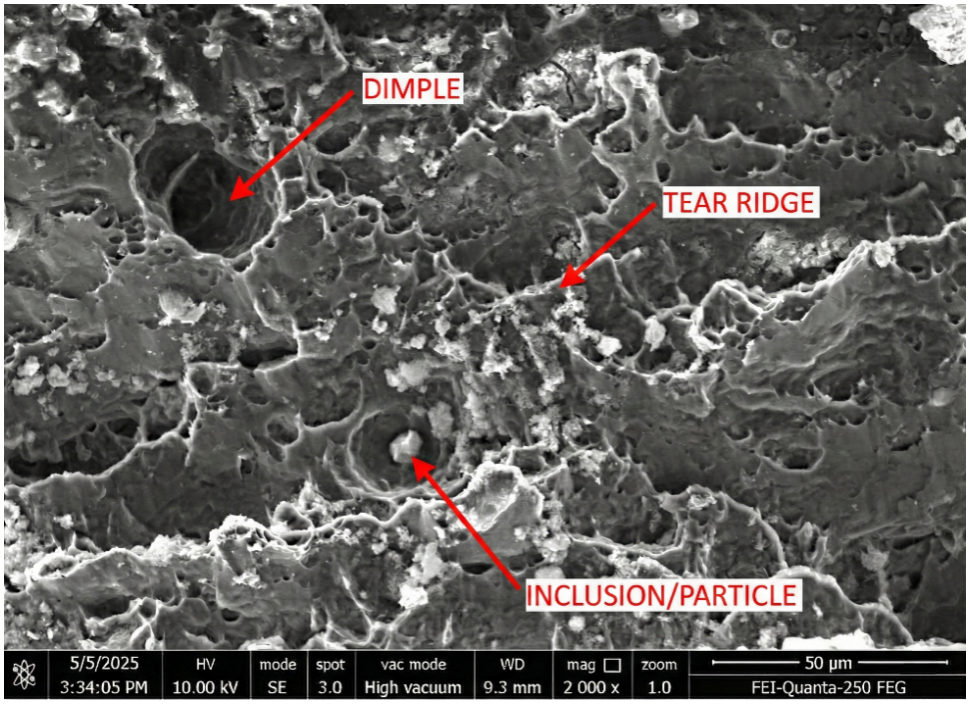

Figure 9. SEM micrograph of the fractured surface of AZ31 Mg alloy formed at the optimal parameters

3.8 ANOVA for Closeness Coefficient

Analysis of Variance (ANOVA) was done to measure the statistical significance of each parameter to the measure of closeness coefficient (CC), which is a composite performance measurement based on TOPSIS. The summarised results presented in Table 6 shows that the major parameters that have an impact on multi-response performance are forming temperature and step-down.

Table 6. ANOVA for Closeness Coefficient, identifying significant factors affecting accuracy.

Factor	Adj SS	Adj MS	F-Value	P-Value	% Contribution
Forming Temperature	0.088707	0.088707	22.17	0.000	34.36%
Step Down	0.080503	0.080503	20.12	0.000	31.18%
Spindle Speed	0.000256	0.000256	0.06	0.802	0.10%
Feed Rate	0.000654	0.000654	0.16	0.690	0.25%
Error	0.088045	0.004002	—	—	

Total	0.258166	—	—	—

Forming temperature ($F = 22.17$, $p < 0.001$) and step-down ($F = 20.12$, $p < 0.001$) are strongly statistically significant, which proves their primary role in the control of deformation behaviour at warm ISF conditions. Their total sum is more than 65% which means that both forming time and forming force are controlled by thermal softening and incremental depth. Conversely, the results shows that spindle speed (p=0.802) and feed rate (p=0.690) produce an insignificant effect, which agrees with the previous main-effects analysis.

The contribution of the error term is attributed to two primary factors. First, it includes the effects of higher-order parameter interactions that are not explicitly separated in the standard orthogonal array design. Second, it reflects the inherent variability in the processes that lead to localized deformation which is typical of warm ISF, such as thermal gradients, frictional variability, and machine compliance. Altogether, the findings of ANOVA confirm that the forming temperature and step-down are the two most important control variables of warm ISF performance, and the spindle speed and feed rate have an insignificant effect within the operating range used. Despite the relatively high error contribution, the F-ratios for temperature and step-down remain statistically significant ($p < 0.05$). This confirms that their identification as the dominant process drivers is reliable and distinct from the experimental noise, even if the precise ranking distinction between the two is marginal.

3.9 Machine Learning–Based Prediction and Validation

A supervised machine learning model was built to complement the results of the experiment and enhance the prediction ability of the key process responses in warm ISF. RFR was selected over simpler linear regression models because the Warm ISF process involves complex, non-linear physical phenomena—such as thermal softening thresholds and strain hardening rates—that linear models fail to capture. While simpler models might yield a smaller train-test gap, they would likely underfit the data.

RFR provides a robust balance, using ensemble averaging to mitigate overfitting while retaining the flexibility to model non-linear process interactions. A Random Forest Regressor (RFR) was modeled using the entire L27 dataset to forecast the forming time, forming force, and the TOPSIS closeness coefficient (CC) with respect to forming temperature in relation to step-down, spindle speed and feed rate. The ML analysis objectives were to (i) confirm that the effects of dominant factors hold, (ii) test the ability to generalise with unseen data and (iii) support the choice of the optimised combination of parameters.

The selection of the Random Forest Regressor (RFR) was driven by a comparative assessment of various machine learning algorithms suitable for the limited dataset (L27) and non-linear process dynamics. Traditional Linear Regression was deemed unsuitable as it fails to capture complex non-linear interactions, such as the threshold-dependent thermal softening of AZ31. Conversely, while Artificial Neural Networks (ANN) are powerful non-linear approximators, they typically require extensive datasets to avoid overfitting and local minima convergence, making them ill-suited for the 27-point experimental design. A Single Decision Tree offers interpretability but suffers from high variance (instability). The Random Forest algorithm overcomes these limitations by employing an ensemble of decision trees (bagging). This approach reduces variance by averaging multiple predictions, allowing it to model complex non-linear boundaries robustly even with a smaller sample size. The model has been trained on an 80:20 train test split, where 200 estimators were used and the maximum depth of a tree was 10. All the response variables have been modelled separately. None of the data transformations were made in such a way that the physical meaning of the measured responses would be retained.

A grid-search algorithm with cross-validation with five folds was used to make sure that the model was stable and was not overfitted during hyperparameter tuning. The search space consisted of 50-300 trees, depth to a maximum of 5-12, and a split/leaf value of 1 to 6 (minimum). The best

set of parameters was 200 trees, maximum depth=10, and min_samples_split=2, which gave the most effective trade off between prediction accuracy and generalisation with the small experimental data. Adding trees beyond 200 did not improve performance meaningfully. Overfitting and worse performance on the test-set occurred with deeper trees (depth greater than 12), but there was no significant improvement in the size of the tree. The chosen 80:20 division was the most predictive and provided enough training. For CC prediction, the Random Forest model achieved a train R^2 = 0.5174 and a test R^2 = 0.4116, corresponding to a train–test gap of approximately 10.6%. This moderate gap indicates that the model is not overfitting and maintains reasonable generalization performance, despite the compounded nature of the CC metric. The reduced fit relative to time and force is expected due to the variance compression associated with TOPSIS normalization and distance-based aggregation. In general, the last Random Forest model proved to be consistent, robust, and adapted to predictive modelling in warm ISF.

3.9.1 Model Performance

Table 7 summarizes the predictive performance of the Random Forest Regressor on the three response variables. The model demonstrated excellent accuracy for the direct physical responses, achieving coefficients of determination (R^2) of 0.9502 for forming force and 0.8675 for forming time. Assessment of overfitting showed that training R^2 and testing R^2 values between forming time (3.4 %) and forming force (2.4 %) showed minimal differences, which translates to excellent generalisation. In contrast, the prediction accuracy for the Closeness Coefficient (CC) was moderate, with an R^2 value of 0.4116. This lower accuracy arises because CC is a compounded metric, unlike force and time which are directly measured physical responses. CC is calculated as a derived index from normalized response matrices and Euclidean separation distances within the TOPSIS framework. This mathematical aggregation introduces nonlinear interactions and compresses the response into a bounded interval [0,1], which inherently reduces variance and makes direct regression more challenging. Nevertheless, the predicted-versus-actual plot in Figure 10(c) shows that the model preserves the relative ranking and trend of the experimental trials, confirming its practical utility for identifying optimal process windows in warm ISF.

Table 7. Random Forest Regression Performance on Test Dataset

Response	R^2	MAE	RMSE
Forming Time (s)	0.8675	1.6304	2.0359
Forming Force (kN)	0.9502	0.0174	0.0214
Closeness Coefficient (CC)	0.4116	0.0409	0.0519

Forming time and forming force have a strong concordance between the predicted and experimental values, as shown in Figure 10(a) and Figure 10 (b). The same can be stated about the predicted-versus-actual plot of CC (Figure 10(c), which is also within the right direction and proves that the multi-response performance ranking is adequately explained by the ML model. The RMSE for forming time (2.0359) is small relative to the variation observed across all trials, and falls within the inherent experimental variability of the process. This demonstrates that the model captures the dominant trends with sufficient precision for practical cycle-time estimation and process planning.

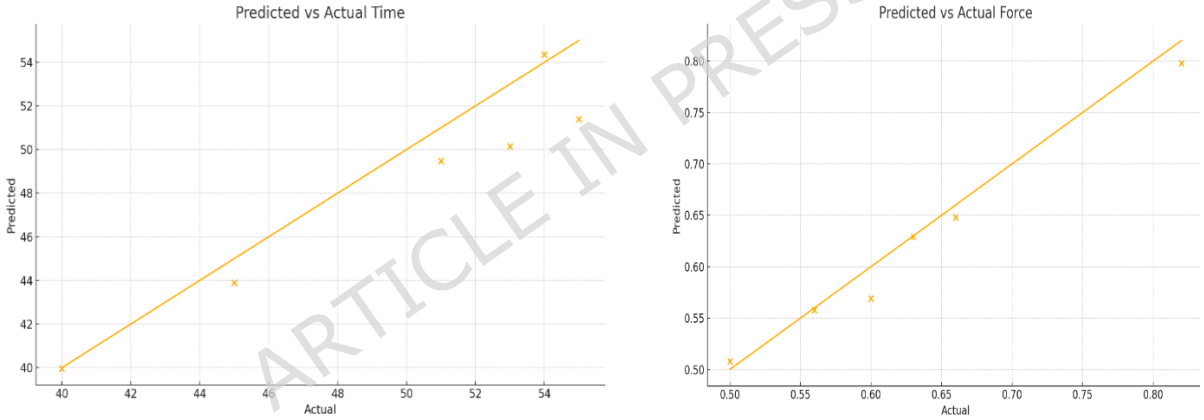

(a)

(b)

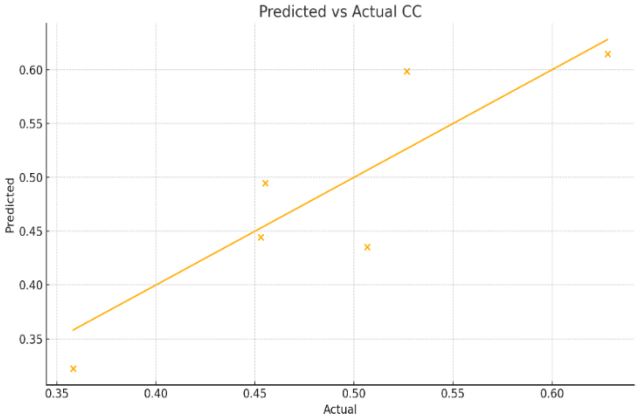

(c)

Figure 10. Performance evaluation of the Random Forest Regression model: Comparison of predicted vs. experimental values for (a) Forming Time, (b) Forming Force, and (c) Closeness Coefficient (CC).

3.9.2 Feature Importance Analysis

The feature importance values were computed using the Gini Impurity (Mean Decrease in Impurity) method. This metric calculates the average reduction in variance brought about by a feature across all 200 trees in the forest. A higher value indicates that the feature is more effective at reducing prediction error at the split nodes, thus serving as a stronger predictor of the process response. The values of the feature-importance obtained with the RFR models are another element of data on the effect of parameters on the data as compared to the standard ANOVA. To establish time, temperature and step-down were the most significant factors, as discussed in Section 3.5 as represented in Figure 11(a).

On the same note, step-down was mainly used in the prediction of forces, with a total contribution of more than 73% of the overall importance (Figure 11(b)). This is consistent with the physical fact that the bigger the incremental depths the more the localised deformation resistance. The second factor was temperature, which supports the importance of temperature in the reduction of the stress of flow in warm forming. In the case of CC prediction, temperature (0.4810) and step-down (0.4488) had almost the same effect, which indicates that they acted jointly and contributed to the multi-response prediction. The effect on Spindle speed and feed rate was again minimal (Figure 11(c)).

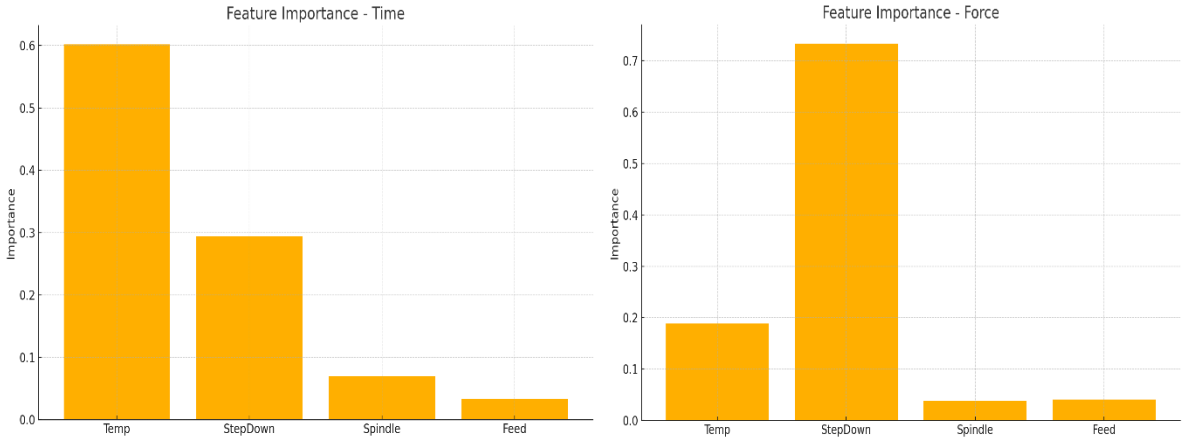

(a) (b)

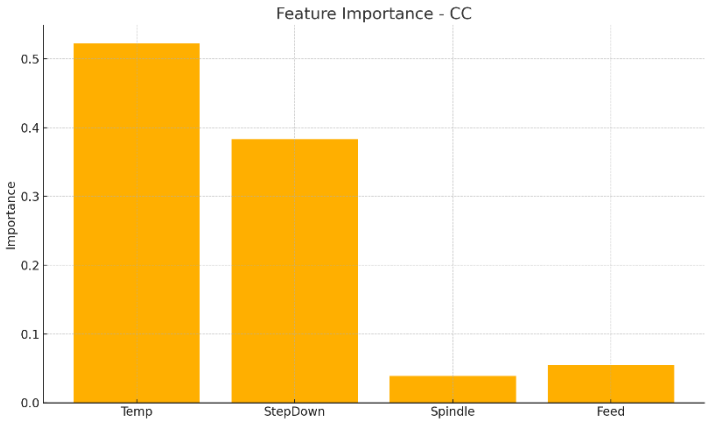

(c)

Figure 11. Feature importance analysis derived from the Random Forest Regressor (RFR) illustrating the relative influence of process parameters on: (a) Forming Time, (b) Forming Force, and (c) Closeness Coefficient (CC).

3.9.3 Discussion and Integration with Experimental Results

The trends in forming time, forming force, and CC of the experiment are also confirmed by the ML analysis: temperature and step-down are always the two dominating parameters in forming. Though the accuracy of CC is moderate, the ML model is able to maintain the overall ranking pattern of experimental trials and proves the validity of the TOPSIS-based multi-response evaluation. The ML findings confirm the fact that the best combination revealed by Taguchi-TOPSIS-250 °C, 0.2 mm step-down, 500 rpm spindle speed, and 750 mm/min feed rate is statistically and computationally justified. The combination of the experimental and machine-learning model forms a strong hybrid predictive-optimiser model to determine the performance of ISF of lightweight AZ31 magnesium alloy sheets.

4. Conclusions

This paper introduced hybrid study, which incorporates experimental design, multi-response optimisation, statistical analysis, machine learning, and fracture-surface testing to examine straight-groove warm ISF of AZ31 magnesium alloy. The main conclusions are as follows: Forming temperature and step-down were found to be the most significant

parameters, indicating 34.35 and 31.18% respectively. Spindle speed and feed rate showed insignificant effect. TOPSIS optimisation was used to identify the most effective combination as Trial 11 and the Taguchi response table suggested the global optimum as 250 °C, 0.2 mm, 500 rpm, 750 mm/min and the predicted CC was 0.6330. These trends were confirmed by a confirmation experiment and gave a forming time = 53 s, a force = 0.483 kN, and a CC = 0.6435 with less than a +5% deviation.

Machine learning with a Random Forest Regressor showed a good predictive power with the results of R^2 of 0.8675 to forming time and 0.9502 to forming force. The statistical findings were validated by feature-importance analysis, in which temperature and step-down were the two most important predictors of the performance of ISF.

SEM fractography showed a complete ductile fracture mechanism, with deep dimples, tear ridges, and void nucleation with the help of inclusions. The microstructural observations are related to the experimental results directly through demonstrating that high temperature favours extensive plasticity, and step-down controls the shear localisation and thinning at the groove wall.

The proposed DOE–TOPSIS–ML–SEM framework offers a scalable and data-efficient methodology for process planning and optimization in warm ISF. From an industrial perspective, the integration of predictive modeling and multi-response optimization can facilitate the adoption of incremental forming in low-volume, customized aerospace, biomedical, and automotive applications. This integrated approach may also be adapted for other lightweight alloys and complex geometries, providing a foundation for smart manufacturing, digital process design, and cyber–physical forming systems.

Funding

The authors received no funding for this work.

Author Contributions

Amar A. Khot, Rohit A. Magdum, Anjali R. Magdum **–** Design and conduct the experiment, Draft manuscript preparation, Data Collection and analysis of results. A.W. Kebede, Pandivelan Chinnaiyan **–** reviewing and editing. All authors reviewed the manuscript.

Data Availability Statement

The datasets generated and analyzed during the current study are available from the corresponding author on reasonable request.

Conflicts of Interest

The authors declare no conflict of interest.

References

1. Park, J. J. & Kim, Y. H. Fundamental studies on incremental sheet metal forming process. *J. Mater. Process. Technol.* **140**, 447–453 (2003).
2. Ambrogio, G., Filice, L. & Gagliardi, F. Warm incremental forming of magnesium alloy AZ31. *CIRP Ann.* **57**, 257–260 (2008).
3. Ben, S. L., Gherissi, A., Thibaud, S. *et al.* Incremental sheet forming: Technology, modeling and formability. *Proc. Inst. Mech. Eng. B J. Eng. Manuf.* **236**, 1916–1943 (2022).
4. Kumar, A. & Trzepieciński, T. Critical review of surface quality in incremental sheet forming. *J. Manuf. Process.* **98**, 767–792 (2024).
5. Schreiber, R. G. & de Jesus, A. M. P. Review of ISF parameters and applications. *Braz. J. Dev.* **8**, 39536–39556 (2022).
6. Gandla, P. K. & Kumar, V. Formability in incremental sheet forming: A critical review. *Results Eng.* **16**, 100615 (2022).
7. Vignesh, G., Narayanan, C. S. & Pandivelan, C. Review on incremental sheet forming process. *J. Manuf. Process.* **56**, 325–348 (2020).
8. An, Z., Yan, D., Qie, J., Lu, Z. & Gao, Z. Warm single-point incremental forming of AZ31 cylindrical parts. *Front. Mater.* **7**, 151 (2020).
9. Ambrogio, G., Filice, L., Gagliardi, F. & Bruschi, S. Incremental sheet forming with local heating of A5083 and AZ31. *Int. J. Mod. Phys. B* **22**, 5601–5607 (2008).
10. Mohanraj, R., Deepak, C. R. & Gokul, V. Warm incremental sheet forming of AZ31 and AA6061. *Proc. Inst. Mech. Eng. B J. Eng. Manuf.* **237**, 1515–1528 (2023).
11. Zhang, H., Li, H., Li, X. *et al.* Influence of temperature in warm incremental sheet forming of AZ31B. *Metals* **11**, 316 (2021).
12. Wang, N. T. *et al.* Robot-assisted cold and warm incremental sheet forming of AZ31. *J. Manuf. Process.* **92**, 654–667 (2023).
13. Trzepieciński, T. & Oleksik, V. Surface finish in single point incremental forming. *Materials* **14**, 1640 (2021).
14. Deokar, S., Shinde, S. & Kumar, S. Incremental sheet forming of non-axisymmetric components. *Procedia Manuf.* **30**, 207–214 (2019).
15. Magdum, R. A. & Chinnaiyan, P. Experimental investigation and optimization of AZ31 magnesium alloy during warm incremental sheet forming. *Coatings* **13**, 68 (2023).
16. Parida, A. K. & Behera, A. Multi-response optimization using TOPSIS. *Int. J. Ind. Eng. Comput.* **5**, 535–546 (2014).

17. Khan, A. A. *et al.* TOPSIS-based multi-objective optimization in hard turning. *Mater. Today Proc.* **46**, 5800–5807 (2021).
18. Kamalizadeh, S. & Karimi, S. TOPSIS approach for milling optimization. *Metals* **12**, 1796 (2022).
19. Kazeem, R. A. *et al.* Multi-process optimization using TOPSIS. *Int. J. Adv. Manuf. Technol.* **130**, 3157–3175 (2024).
20. Rawat, S. & Singh, R. Enhanced TOPSIS for multi-objective optimization. *Expert Syst. Appl.* **244**, 123116 (2024).
21. La, N. T. *et al.* Hybrid Taguchi–TOPSIS optimization in ultrasonic incremental forming. *Materials* **17**, 2152 (2024).
22. Chinnaiyan, P. & Jeevanantham, A. K. Multi-objective optimization of single point incremental sheet forming of AA5052 using Taguchi based grey relational analysis coupled with principal component analysis. *Int. J. Precis. Eng. Manuf.* **15**, 2309–2316 (2014).
23. Patel, D. M. & Gandhi, A. H. Experimental investigation and optimization of forming parameters in single point incremental forming of AZ31 magnesium alloy. *Int. J. Exp. Res. Rev.* **46**, 240–252 (2024).
24. Maji, K. & Kumar, G. Inverse analysis and multi-objective optimization of single-point incremental forming of AA5083 aluminum alloy sheet. *Soft Comput.* **24**, 4505–4521 (2019).
25. Xie, Z.-D. *et al.* Effects of ultrasonic vibration on performance and microstructure of AZ31 magnesium alloy under tensile deformation. *J. Cent. South Univ.* **25**, 1545–1559 (2018).
26. Van Sy, L. & Thanh Nam, N. Hot incremental forming of magnesium and aluminum alloy sheets by using direct heating system. *Proc. Inst. Mech. Eng. B J. Eng. Manuf.* **227**, 1099–1110 (2013).
27. Ostasevicius, V. *et al.* Machine learning methods for single point incremental forming process monitoring. *Sensors* **21**, 18 (2021).
28. Harfoush, A., Vanhoucke, B. & Duflou, J. R. Artificial intelligence in incremental sheet forming. *Procedia Manuf.* **54**, 21–28 (2021).
29. Möllensiep, D., Liu, S. & Tekkaya, A. E. ANN-based prediction of geometric accuracy in incremental sheet forming. *Int. J. Adv. Manuf. Technol.* **135**, 4021–4035 (2024).
30. Wang, C. *et al.* Learning-based model predictive control for incremental sheet forming. *J. Manuf. Syst.* **69**, 315–329 (2023).
31. Kurra, S., Regalla, S. P. & Gupta, A. K. Prediction of surface roughness using machine learning technique for incremental sheet forming process. *J. Mater. Eng. Perform.* **31**, 4512–4525 (2022).
32. Mittal, A. *et al.* Machine learning enabled estimation of formability for anisotropic sheet metals. *Int. J. Mech. Sci.* **265**, 108845 (2024).
33. Liu, Z. *et al.* Study on incremental sheet forming performance of aluminum alloy based on adaptive fuzzy PID temperature control. *Metals* **12**, 852 (2022).

34. Li, W., Shu, C., Hassan, A. *et al.* Application of machine learning on tool path optimisation and cooling lubricant in induction heating-assisted single point incremental sheet forming of Ti-6Al-4V sheets. *Int. J. Adv. Manuf. Technol.* **123**, 821–838 (2022).
35. Li, H. *et al.* Machine learning for predicting fracture strain in sheet metal forming. *Metals* **12**, 1799 (2022).
36. Do, V. C. *et al.* Enhancing forming limit curve and fracture height predictions in single-point incremental sheet forming of sheet material. *Materials* **16**, 7306 (2023).
37. Xiao, X. *et al.* RSM and BPNN modeling in incremental sheet forming process for AA5052 sheet: Multi-objective optimization using genetic algorithm. *Metals* **10**, 1003 (2020).
38. Zhang, W. *et al.* Microstructure evolution and mechanical properties of AZ31 magnesium alloy sheets prepared by low-speed extrusion with different temperature. *Crystals* **10**, 644 (2020).
39. Sevšek, L. *et al.* Soft computing for SPIF process parameter correlation. *Appl. Soft Comput.* **141**, 110497 (2023).
40. Magdum, R. A. & Chinnaiyan, P. A critical review of incremental sheet forming in view of process parameters and process output. *Adv. Mater. Process. Technol.* **8**, 2039–2068 (2022).
41. Guo, J. *et al.* Wire arc additive manufacturing of AZ31 magnesium alloy: Grain refinement by adjusting pulse frequency. *Materials* **9**, 823 (2016).
42. Qin, Z., Gatea, S. & Ou, H. Friction and heat partition coefficients in incremental sheet forming process. *J. Manuf. Process.* **124**, 503–523 (2024).
43. Xu, J. *et al.* Microhardness, microstructure and tensile behaviour of an AZ31 magnesium alloy processed by high-pressure torsion. *J. Mater. Sci.* **50**, 7424–7436 (2015).